A simple vortex model of a thunderstorm downburst – a parametric evaluation

Mike Jesson and Mark Sterling

University of Birmingham, Edgbaston, Birmingham, UK

ABSTRACT: Thunderstorm downbursts are short-lived, transient extreme wind events which can cause wind speeds equivalent to a category EF3 tornado (~150mph). The complex flow field which they produce has previously been the subject of time-expensive numerical modelling. However, it is well-known that there is a large, random variation in full-scale downbursts and so a quick, easily varied model would be of benefit to engineers calculating dynamic loading on structures. This paper introduces a simple and computationally inexpensive vortex model of a downburst, which is shown to model the main features of the flow field in a physically simulated thunderstorm downburst to an appropriate degree of accuracy.

KEYWORDS: Transient winds, numerical model, vortex, thunderstorm, downburst, wind engineering.

1 INTRODUCTION

A thunderstorm downburst is a transient, highly localised extreme wind event which can cause wind speeds of 150mph, equivalent to a category EF3 tornado ([1]). These events are created by the cooling of (and precipitation within) warm, moist, rising air in a convective thunderstorm cell, which then reverses direction to form a downdraft which impinges on the ground. A primary ring vortex forms around the downdraft, and is carried radially outwards with the outflow from the impingement point. The superposition of the outflow and vortex flow fields creates a region of very high wind speed. Numerical simulations also indicate the development of a smaller, secondary vortex at the base of the primary ([2], [3]), caused by the interaction of the flow and ground roughness. The combination of these flow elements results in a flow field which is very different from that seen in atmospheric boundary layer (ABL) flows. Unlike ABL winds, which for the purposes of design are regarded as statistically stationary over a number of hours and uniform over tens of kilometres, downbursts typically have a lifetime of only a few minutes (Figure 1) and a downdraft radius of approximately 1 – 2km. The vertical distribution of radial wind-speed typically has a peak maximum (u_m, the spatio-temporal maximum over the whole flow field) close to the ground, at a height (z_m) of 30 – 100m (Figure 2; [4], [5]). One feature of downbursts is the variability of such events, with no two recorded downbursts producing precisely the same flow fields ([6]–[8]), although there are clear similarities between the large-scale characteristics.

There is growing consensus that extreme weather events such as downbursts may become more frequent due to climate change. Consequently, efforts have been made to understand the wind loading which they exert. Due to the difficulty in predicting where and when a downburst will

occur, along with the usual issues of variability, the use of full-scale measurements for the determination of downburst wind loading is problematic (though the work of Lombardo ([7]) provides a very useful data set for validation). For this reason, simulations are used to model downbursts and (in some cases) their effects on structures, both physically (e.g. [9]–[14]) and numerically ([3], [15], [16]). The more advanced physical simulators, such as that used by McConville et al. ([17]) and Jesson et al. ([12], [13]), model the transient nature of a downburst event, and exhibit the same run-to-run variation which has been seen as with full-scale events ([17]). This variation limits the insight which can be gained, although general loading patterns may be quantified (e.g. [12], [13]). On the numerical side, techniques such as Large Eddy Simulation and cloud models have been used, with the lifecycle of the downburst being simulated from the initial downdraft to the formation and motion of the ring vortex. Although they are of importance in elucidating the mechanisms which drive a downburst and lead to their high wind speeds, these techniques are computational expensive. Holmes and Oliver [18] suggested a simple empirical model, based around a time-varying impinging jet profile. Arguably, this model lacks a clear relationship to the components making up the complex flow field, and therefore does not suitably model vertical variation.

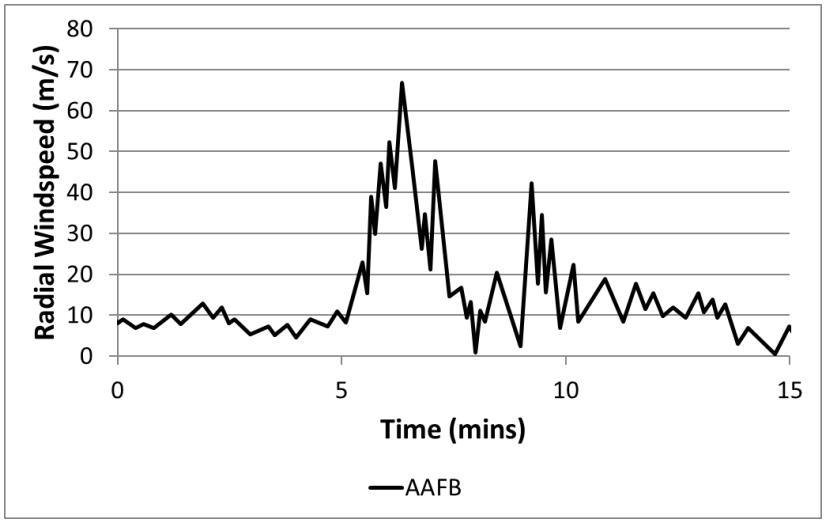

Figure 1: Radial wind-speed time-series from the Andrews Air Force Base downburst event, 5m above ground (adapted from [1])

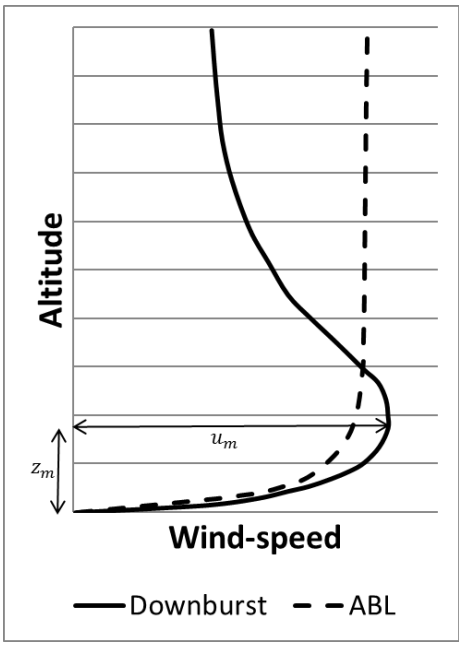

Figure 2: Schematic vertical distribution of velocity for a downburst and ABL flow. u_m is the maximum radial wind-speed of the downburst, z_m is the altitude at which this wind-speed occurs (adapted from [5]).

A simple numerical model of a downburst is presented in this paper. Before presenting the model definition, a brief description of the University of Birmingham Transient Wind Simulator (UoB-TWS) is given in Section 2; experimental data from the UoB-TWS provides the reference data for model validation. The model, which is described fully in Section 3, calculates the velocity field as a superposition of a primary vortex, secondary vortex and linear outflow velocity. Section 4 compares model output with the UoB-TWS data, and includes a parametric study which identifies the important parameters in defining and creating a downburst flow field. Finally, important conclusions from this work are presented.

2 UNIVERSITY OF BIRMINGHAM TRANSIENT WIND SIMULATOR (UOB-TWS)

The UoB-TWS is a vertical impinging jet downburst simulator with a length scale estimated as 1:1600 and is described fully by Jesson et al. ([12], [13]). Aperture control is used to simulate the rapid flow accelerations which occur in full-scale downbursts and the simulator has been shown to simulate the transient aspects of a downburst flow ([12], [13], [17]). Run-to-run variation is seen in the simulations, as has been noted in full-scale events and mentioned in the introduction. In order to investigate the generic aspects of downbursts, while minimising the effects of such variation, an ensemble-mean approach has been used in analysing the UoB-TWS data. Thus, time-series from multiple runs are averaged according to:

$$u(t) = \frac{1}{N}\sum_{n=1}^{N} u_n(t) \quad (1)$$

where $u(t)$ is the ensemble-mean velocity time-series, n is the run index, N is the total number of runs in the ensemble and $u_n(t)$ is the velocity time-series from the n^{th} experimental run. Ensemble-mean values are used in this paper.

The aim of the original UoB experiments was to measure the wind loading on building models in a simulated downburst. The velocity measurements had two purposes: Firstly, to identify the position, (x_m, z_m), of the peak maximum outflow velocity (found to be $x_m/D = 1.50$, $z_m/D = 0.02$), where x is the radial distance from the centre of the downdraft, z is the vertical position and D is the diameter of the simulated downdraft and *m* denotes a maximum), and secondly to ensure that the vertical profile of radial velocity at this point was consistent with full-scale data (which was demonstrated by comparison with the work of Hjelmfelt ([5]; see [13])). Velocity measurements were made at 10mm vertical spacings for profiles measured at $x/D = 1.00$, 1.50, 2.00 and 2.50, with partial profiles (vertical positions around z_m only) at $x/D = 1.25$ and 1.75 to verify that the $x/D = 1.50$ profile included the maximum velocity point.

3 THE VORTEX MODEL

3.1 *Model Development*

An early version of the vortex model has been presented by Jesson and Sterling ([19]) and this description is expanded and updated here. A non-translating downburst is simulated, i.e., the downburst is not part of a larger storm which carries the downburst with it (although incorporating the translation of the storm would be relatively straightforward). This permits the assumption that the downdraft creates an axially symmetric outflow around the impingement point, meaning that model is 2-D within a cylindrical polar coordinate system; variation occurs along the radial (x) and vertical (z) directions only. The respective velocities are u and w, and the velocity field is assumed to be the superposition of three, independent velocity fields, one from each of the main flow structures:

- The main outflow from the downdraft impingement point.
- The primary ring vortex.
- The secondary vortex.

This superposition is a technique applied in (inviscid) potential flow models, as is the use of mirrored vortices (Figure 3) to ensure that the condition of zero flow across the ground plane is met. The mirroring of the vortices also accelerates the radial flow close to the boundary, as required by continuity to reflect the contraction of the flow field by the ground plane. Radial motion of the vortices is governed purely by the outflow velocity (a model parameter; vertical motion is a

separate model parameter, as discussed later). In standard potential flow theory, the flow is assumed to be inviscid, leading to vortices with a singularity at the centre. In this model, each vortex is an independent (viscous) Rankine-type vortex. For a circular Rankine vortex with a core of radius R and circulation Γ, the tangential wind speed at a radial distance r from the centre, $V_\theta(r)$, is given by:

$$V_\theta(r) = \begin{cases} \dfrac{\Gamma r}{2\pi R^2} = \dfrac{\Gamma\sqrt{X^2+Z^2}}{2\pi(X_R^2+Z_R^2)} for\ \ r \le R \\ \dfrac{\Gamma}{2\pi r} = \dfrac{\Gamma}{2\pi\sqrt{X^2+Z^2}} for\ \ r > R \end{cases} \quad (2)$$

where, in the Cartesian form, (X, Z) is a general point in the domain, (X_R, Z_R) lies on the core boundary, and capitals indicate a local coordinate system with its origin at the vortex centre (Figure 4).

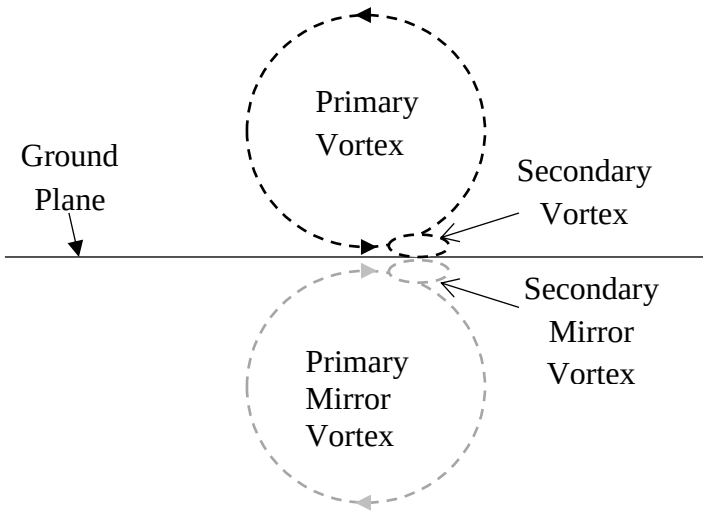

Figure 3: Schematic application of mirrored vortices.

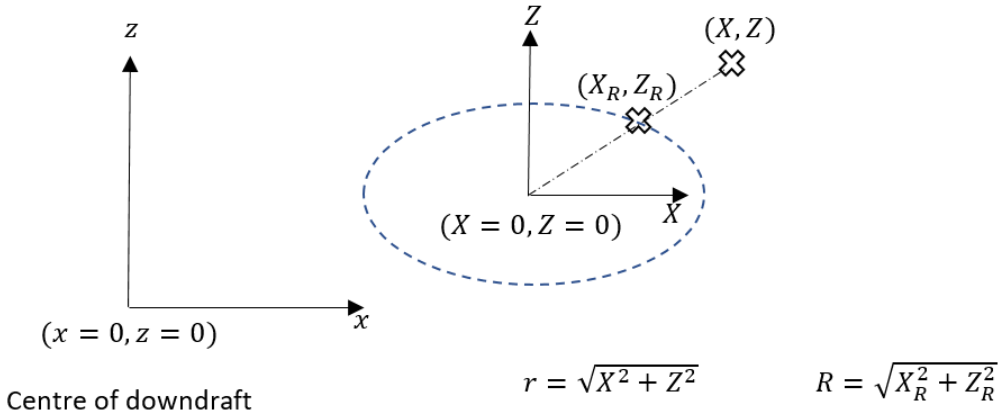

Figure 4: Definition of the coordinate system.

In order to estimate the relative positions and speeds of the three elements of the flow field, reference was made to rudimentary flow visualisation work at the University of Birmingham ([17], [20]) and the numerical work of Mason ([3]) and Kim & Hangan ([2]). From these it was observed that:

- The primary vortex changes shape (becoming elliptical) and weakens (reducing circulation) with time, i.e. as it spreads out from the centre of the impingement zone. In addition to the reduction in circulation, it also lifts from the ground.
- The secondary vortex is initially not present, but strengthens with time before weakening. It forms at the leading edge of the primary vortex, at ground level but, according to Mason's CFD simulations, ([3]) is lifted by the rotation of the primary vortex.

The vortex model outlined in this paper, includes parameters to govern the initial size, shape, position and strength of each vortex, and also the rate of change of these parameters. For the secondary vortex, a "half-life" can be configured, such that the magnitude of the vortex increases up to the half-life, following which the vortex weakens. The full list of parameters is given in Table 1.

The evolution of the vortices from circular to elliptical has been incorporated in the model through specifying the rate of change of the length of the ellipse axes, one of which is parallel to the x-axis and the other parallel to the z-axis. The circumference of the vortex core is thus defined by:

$$\frac{X_R^2}{a(t)^2} + \frac{Z_R^2}{b(t)^2} = 1 \tag{3}$$

where $a(t)$ and $b(t)$ are the lengths of the principal axes, which vary with time, t. $V_\theta(r)$ is then calculated using a modified version of (2) such that r is the distance along the line joining

the centre of the ellipse and the point at which the velocity is calculated, and R is the ellipse radius along that line (Figure 4).

Table 1 Vortex model parameters.

Parameter	"Best Fit"	
	Primary Vortex	**Secondary Vortex**
Initial circulation (m^2/s)	18.00	0.00
Rate of change of circulation (m^2/s^2)	-35.00	-7.00
Initial x, z radii (m)	0.30, 0.30[a]	0.08, 0.005[e]
Rate of change of x, z radii (m/s)	0.10, -0.02[c&e]	0.00, 0.02[c&e]
Initial centre position, x, z (m)	0.80[b], 0.30[b]	0.88[d], 0.005[e]
Translation speed, x, z-directions (m/s)	Varies[f], 0.00	Varies[g], Varies[e]
Half-life (s)	N/A	0.20
Final Outflow Velocity (m/s)	10.00	
Time Step (s)	0.01	
Grid Spacing* (m)	0.25	

*Grid spacing does not affect the values calculated for each grid node.
Superscript letters indicate parameters which, for the determination of the Best Fit, are calculated from other parameters according to the referenced assumption(s) detailed in Section 3.2.

3.2 *Parameter Quantification*

Values for the model parameters were initially estimated from the references stated above, and then refined to improve the fit of the model to the UoB-TWS data while ensuring that the values remained representative of the reference data. The refinement process involved incrementing model parameters over multiple runs and then identifying the "best fit" configuration. In order to make the number of runs manageable (by reducing the number of varied parameters and hence parameter combinations) it was assumed that:

a) The primary vortex is initially circular.
b) The primary vortex always starts with its bottom edge touching the ground plane and its rear edge touching the edge of the downdraft region (i.e., the initial position is a function of the initial size, and does not vary independently; the vortex "edge" is at radius R).
c) The combination of the rate of change of z-radius and z-translation speed is such that $R = 0.02m = z_m$ when the secondary vortex has its greatest circulation.
d) The secondary vortex starts with its rear edge at the centreline of the primary vortex.
e) At its vertical centre, the secondary vortex spans the distance between the ground plane and the primary vortex.
f) The translation speed is the outflow speed. This is initially zero, but increases to the final outflow velocity in a time of 1.6 times the secondary vortex half-life. The factor of 1.6 was estimated as resulting in the outflow velocity reaching its maximum as the rear of the vortex

passes x_m, and variation of this factor (not shown) demonstrates that the chosen value gives the best fit to the experimental data.

g) The secondary vortex moves horizontally at the same speed as the primary vortex. No relative motion has been included in this version of the model.

Note that these assumptions were only applied for the evaluation of the best fit, and not for the parametric variation presented in Section 4.2.

Configurations for which the peak maximum velocity did not occur at $x/D = 1.50$ and $0.01 \leq z/D \leq 0.04$ (as seen in the UoB data), or for which the peak maximum velocity was more than $\pm 0.1 m/s$ from the experimental value were discarded. For the acceptable configurations, "Best Fit" was evaluated using the root mean square (RMS) difference between the UoB experimental data and the model output. The data used for this calculation included the vertical profiles of local maximum radial velocity at $x/D = 1.00$, 1.25, 1.50 and 1.75, and also the velocity time-series at the position of maximum radial velocity. The vertical profile at $x/D = 2.00$ and 2.50 were not used for reasons discussed below.

The Best Fit values for the model parameters are given in Table 1.

4 RESULTS AND DISCUSSION

4.1 *Best Fit*

Using the Best Fit model parameters shown in Table 1, the vertical profiles of radial velocity have been calculated for the same radial positions as were used for the non-translating UoB-TWS experiments (Figure 5), and the time-series calculated at the position of global maximum radial velocity (Figure 6). For $x/D \leq 1.75$ the experimental data are modelled well by the Best Fit profiles – with the exception of the $x/D = 1.50$ profile at $z/D = 0.01$ data (discussed below) and isolated points above $z/D = 0.15$ (equivalent to 800m full-scale), all data fall within envelope of individual run values. As the secondary vortex strengthens the "nose" of the typical downburst vertical profile becomes evident. Beyond this position, the vortices decay rapidly in the physical simulations, a decay not accurately modelled by the vortex model (for this reason, these vertical sections were not used for the best fit calculation outlined in Section 3.2). Another difference is in the vertical spread of the "nose", which spans the lowest three data points in the UoB-TWS data. The vortex model creates a sharp nose where the outflow velocities from the two Rankine-type vortices combine; each vortex will have a clearly defined radius of maximum tangential velocity, resulting in this sharply defined, high-speed region. It is possible that the interaction of the primary and secondary vortices is distorting the flow field in this region, making the Rankine-type model inappropriate. Notwithstanding these differences, the vortex model is shown to give a good representation of the flow field over the main region of interest, from the edge of the downdraft to the radius of maximum velocity and slightly beyond.

At the point of global maximum radial velocity, the model also captures the main features of the velocity time-series (Figure 6). The initial acceleration is slightly lower (~5%) in the vortex model, with a narrower peak (~30%). The deceleration phase from the model also matches the

experimental data, with the final outflow velocity matched. The narrower peak may be due to the simplifications and assumptions made in the position and motion of the secondary vortex (which is not modelled as moving up and around the perimeter of the primary vortex, indicated by Mason et al. ([3])). Incorporation of these more complex relationships may be included in future model development.

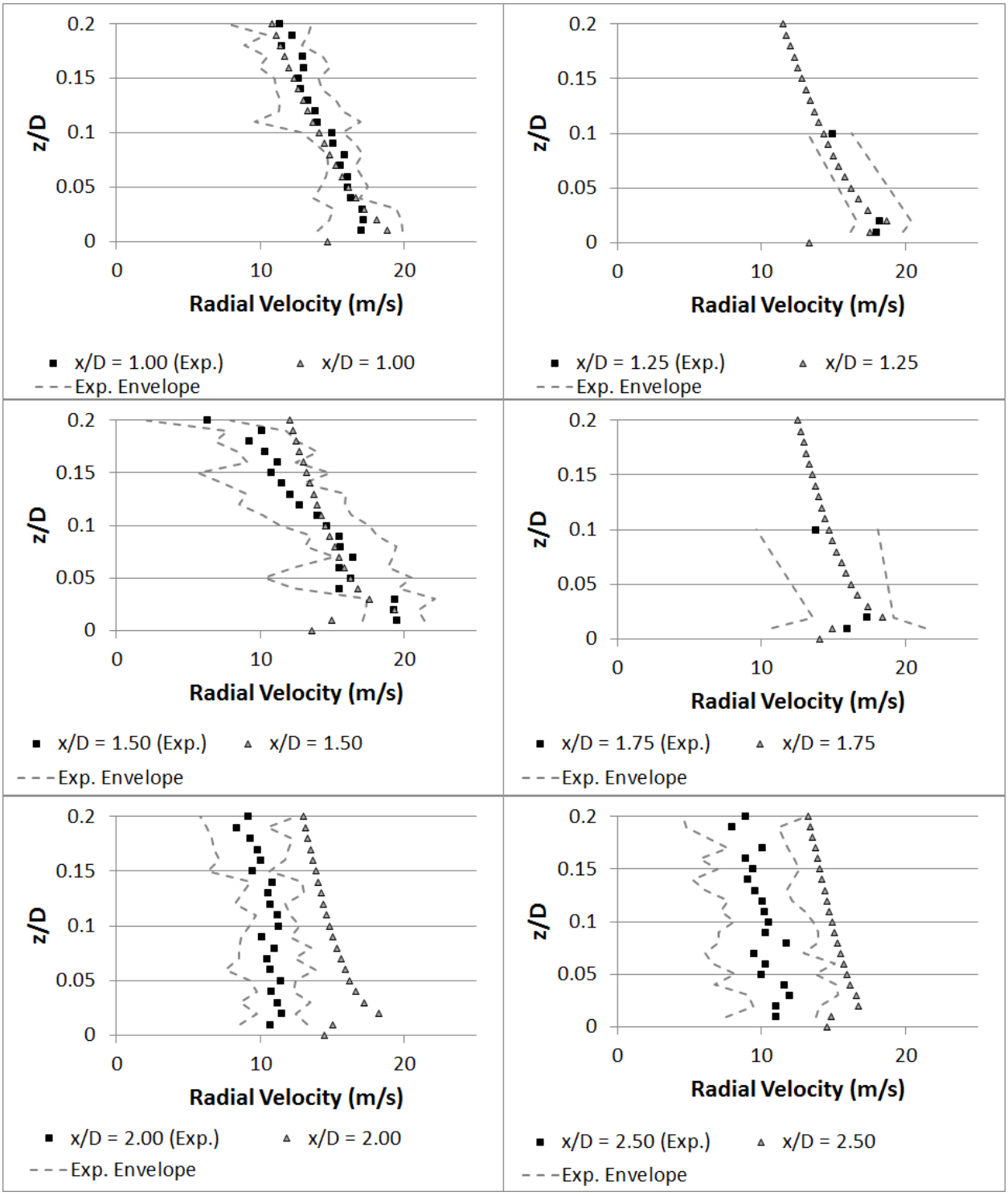

Figure 5: Comparison of vortex model Best Fit output with UoB-TWS experimental data ("Exp."). The experimental envelope is the upper and lower bounds of the individual run velocities at the time of the ensemble maximum.

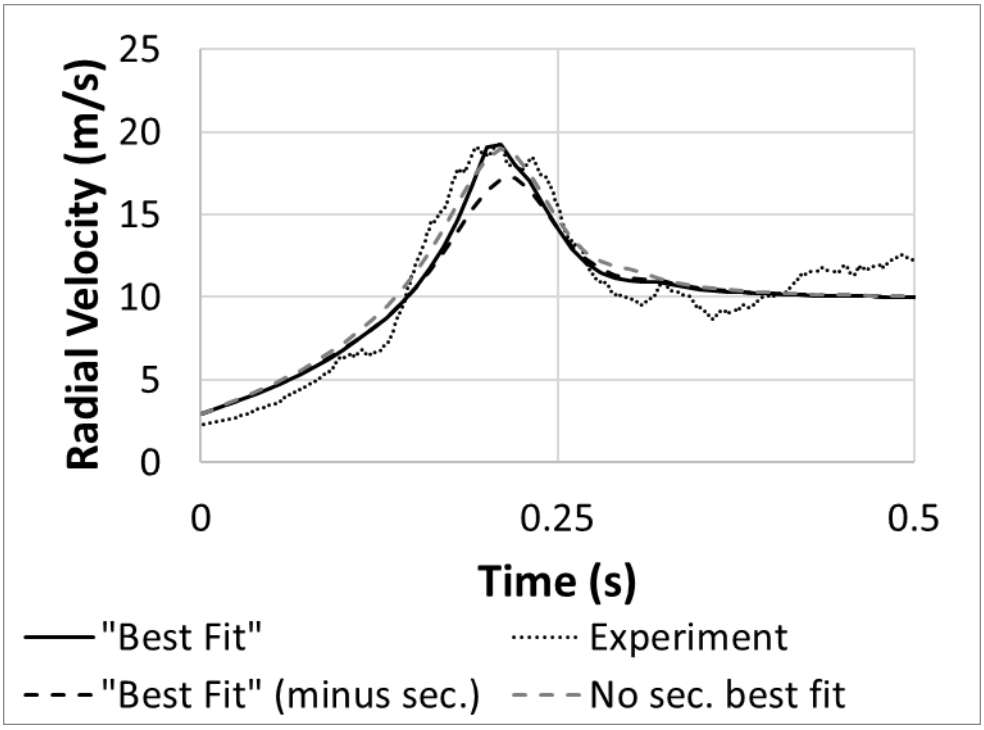

Figure 6: Model and experimental radial velocity time-series at the point of the global maximum velocity in the UoB experiments. '"Best Fit" (minus sec.)' uses the Best Fit parameters except with no secondary vortex. 'No sec. best fit' is the best fit obtained if there is no secondary vortex and other parameters are varied.

4.2 *Parametric Study*

In order to assess the importance of the secondary vortex, the model was run using the primary vortex parameters from the Best Fit configuration but no secondary vortex. The model was also run to determine the best fit achievable with no secondary vortex. In the former case, the maximum radial velocity is approximately 11% lower ($17.2m/s$ rather than $19.3m/s$), and the acceleration is reduced (Figure 6). In the latter case, the velocity time-series at $x/D = 1.50$ is negligibly different from the Best Fit series. However, examination of the vertical distributions of the radial velocity component (Figure 7 and Figure 5) shows the importance of the secondary vortex, which is responsible for the development of the profile close to the ground and the prominent "nose" of the typical downburst profile.

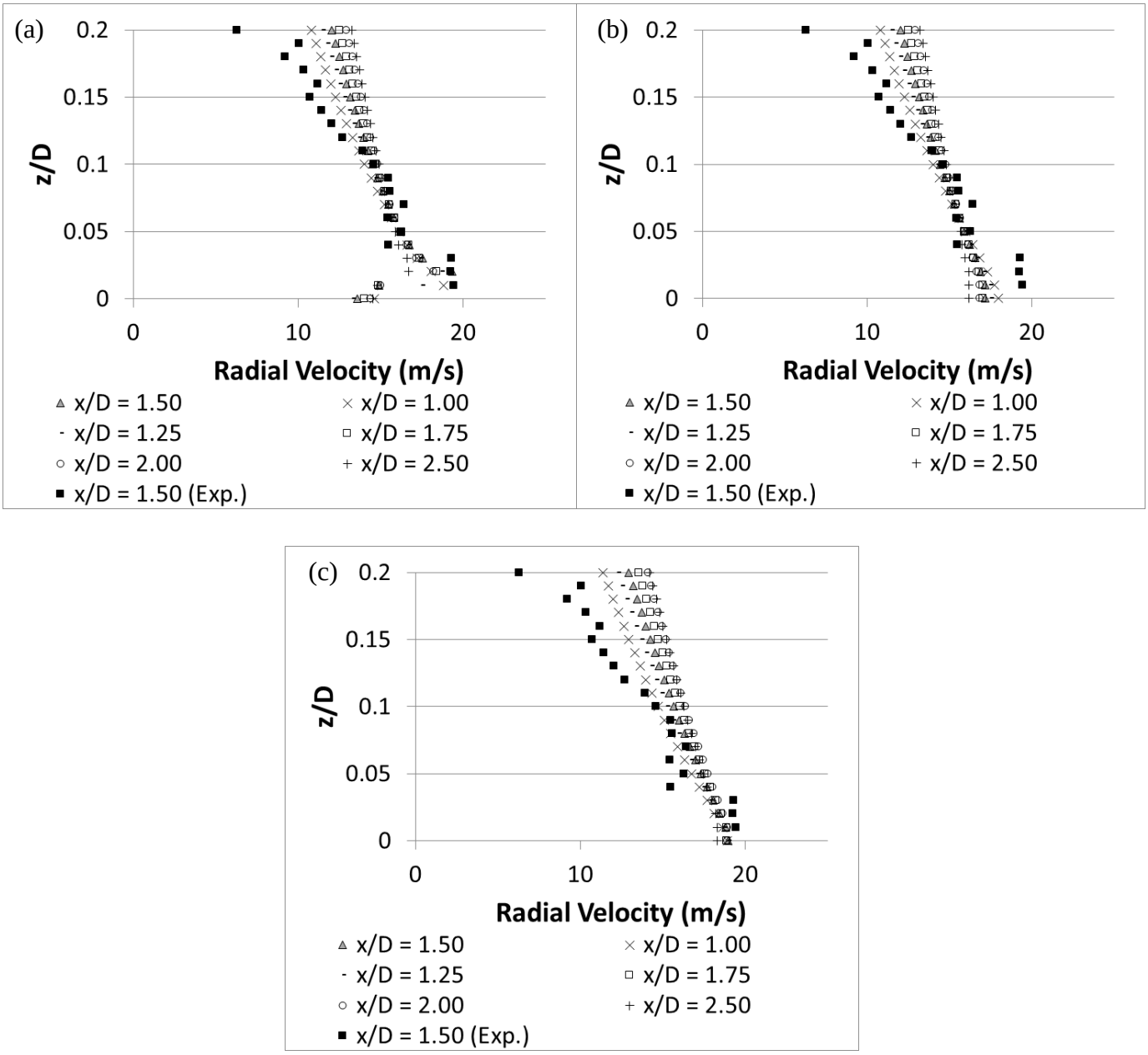

Figure 7: Vertical distributions of radial velocity for (a) Best Fit configuration, (b) configuration as for Best Fit configuration but with no secondary vortex, and (c) the best fit found if no secondary vortex is permitted.

Using the Best Fit parameter values as a baseline, each parameter was varied in turn in order to quantify the sensitivity of the model output to that parameter. Variations of -25%, -10%, +10% and +25% of the Best Fit value were used. Only parameters for which the variation had a significant effect on the model output are discussed here. Variation of the primary vortex initial circulation (Figure 8) changes the magnitude the vertical profile of radial velocity while maintaining the same qualitative profile, with the maximum radial velocity varying approximately linearly with the circulation. Changing the initial circulation of the primary vortex does not change

the relative positions of the primary and secondary vortices, nor does it change the relative rate of change of the two circulations (due to the assumption made in section 3.2), thus the position of the peak maximum radial velocity is unchanged by changing the initial circulation. The rate of change of primary circulation has a smaller effect (9% change in u_m for a 25% parameter change), and the variation is inversely, linearly proportional (Figure 9). The inverse law would be expected due to this rate of change being negative (i.e. a weakening vortex) and so a percentage increase accelerates the weakening.

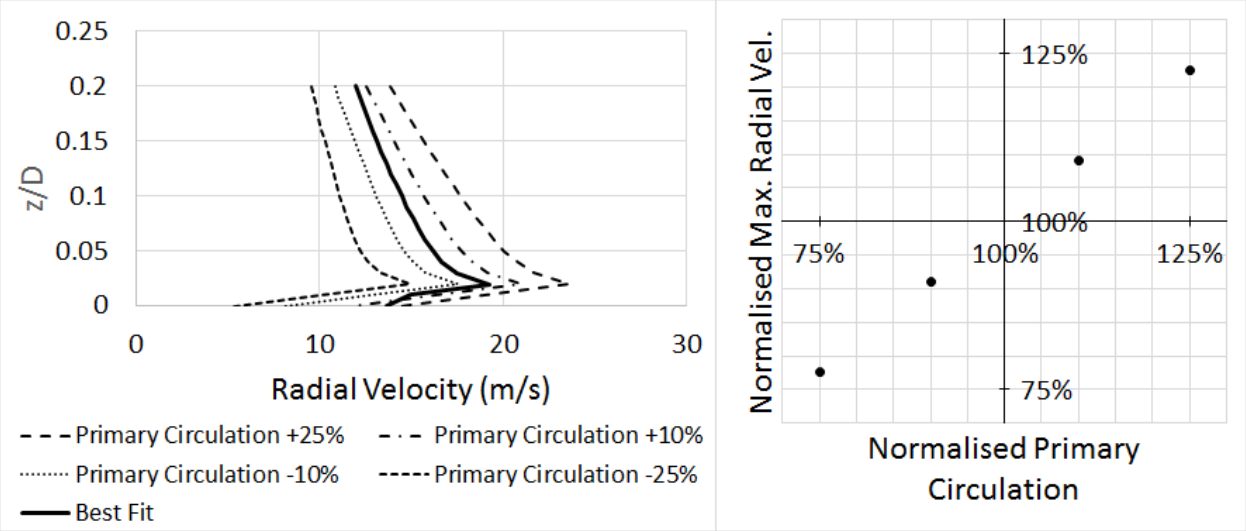

Figure 8: Effect of varying the primary circulation. Vertical profile of radial velocity at $x/D = 1.50$ and normalised variation. Normalisation is by the Best Fit value.

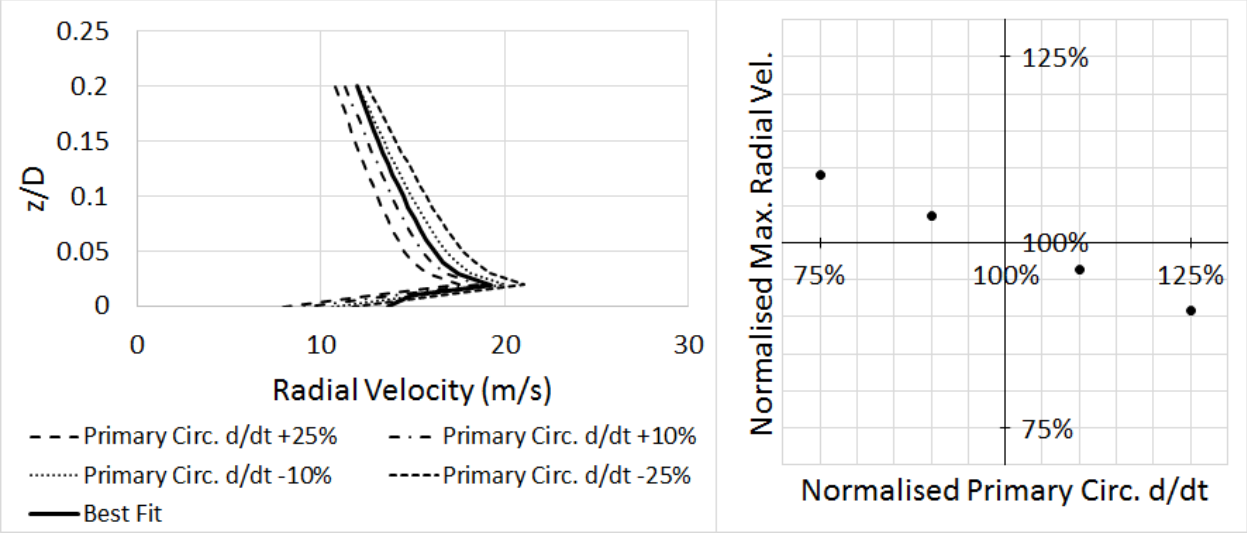

Figure 9: Effect of varying the rate of change (d/dt) of the primary circulation. Vertical profile of radial velocity at $x/D = 1.50$ and normalised variation. Normalisation is by the Best Fit value.

The initial secondary circulation is zero, as required by the hypothesised method of its formation, and so its variation has not been considered. Further, realistically sized variations of

the rate of change of secondary vortex circulation have negligible effect on u_m or z_m. The impact of varying the half-life of the secondary vortex is more complex. With a shorter half-life, the secondary vortex reaches its maximum circulation more quickly. Consequently, the primary vortex has a greater circulation at this instant, and (with the rate of change of the secondary vortex radii being positive) the secondary vortex is smaller than at later times, resulting in a higher velocity for the same circulation. This latter point is, arguably, an artefact of the model rather than necessarily representative of the physical system. The result of this is an increase in u_m as the half-life decreases, and the maximum velocity at $x/D = 1.50$ occurring earlier (Figure 10). This change in u_m is non-linear due to the complex relationship between u_m and the instantaneous strengths of both vortices – an increase of the same percentage results in a larger magnitude change than the corresponding decrease (Figure 10). The time of occurrence, and therefore radial location, of u_m is also dependent on the half-life; for a 25% increase in the half-life u_m occurs at $x/D = 1.00$, while for a 25% decrease it remains at $x/D = 1.50$ (not shown).

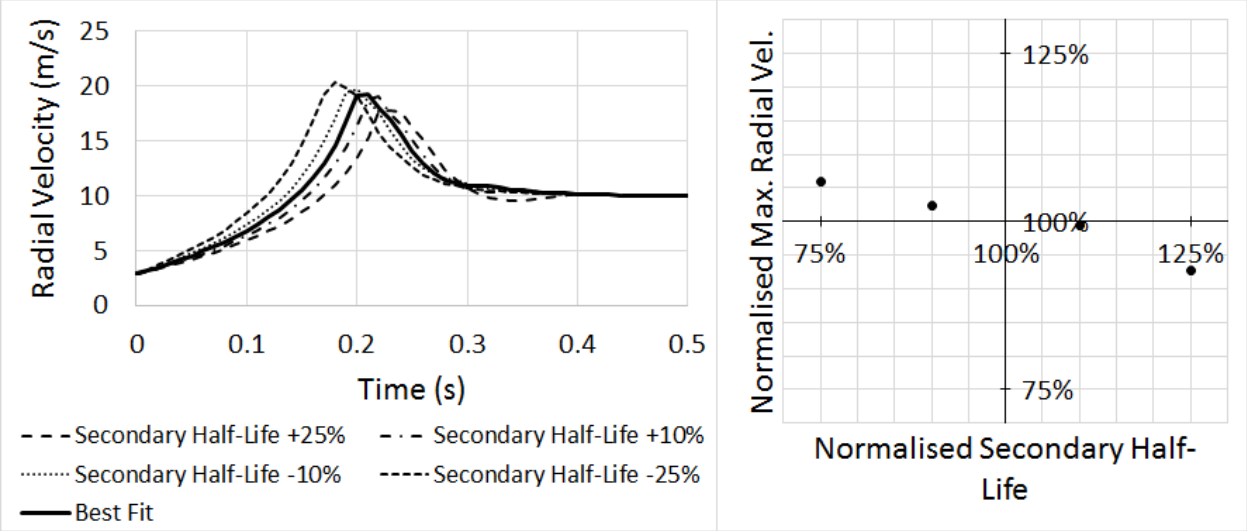

Figure 10: Effect of varying the half-life of the secondary vortex. Radial velocity time-series at $x/D = 1.50$ and normalised variation. Normalisation is by the Best Fit value.

Increasing the initial x-radius of the primary vortex increases the width of the time-series peak (Figure 11). On first inspection, this may appear to give opportunity to further refine the model output, due to the Best Fit peak being narrower than shown in the experimental data (Figure 6). However, the broadening of the peak around the time of maximum velocity is limited, and the additional size of the vortex also increases the initial velocity at $x/D = 1.50$, reducing the acceleration phase of the outflow. Due to possible overshoot effects, modelling this acceleration phase is arguably more important than widening the peak to match the plateau in the experimental data.

Moving the starting x-position of the primary vortex (which is, by assumption (Section 3.2), with the rear edge of the vortex at the edge of the downdraft region) towards the centre of the

downdraft is physically unrealistic. Conversely, it is conceivable that the primary vortex will start a distance away from the downdraft edge, with the downdraft almost certainly not being a perfect circle as is generally assumed. Due to the design of the model, such a variation would only have the effect of shifting x_m, the radial position of u_m, by an equivalent amount and so this will not be discussed further. Of more interest is the starting position of the secondary vortex, as this will be determined by the precise mechanism of its formation and, likely, the roughness of the ground the downburst forms over. Variation of this parameter shows a decrease in the maximum velocity at $x/D = 1.50$ (Figure 12) for both an increase and decrease. Increases show a proportionally larger reduction, though again the changes are small relative to those caused by a change in the primary circulation. Further, for increases in the secondary starting x-position, x_m moves towards the downdraft region, with u_m occurring at $x/d = 1.00$ for a 25% increase. Again, due to the interaction of the primary and secondary vortices, and their rates of strengthening/decay, there is no clear pattern for the change of x_m. For a 10% decrease in secondary starting x-position $x_m/D = 1.25$ but for a 25% decrease it reverts to $x/D = 1.50$.

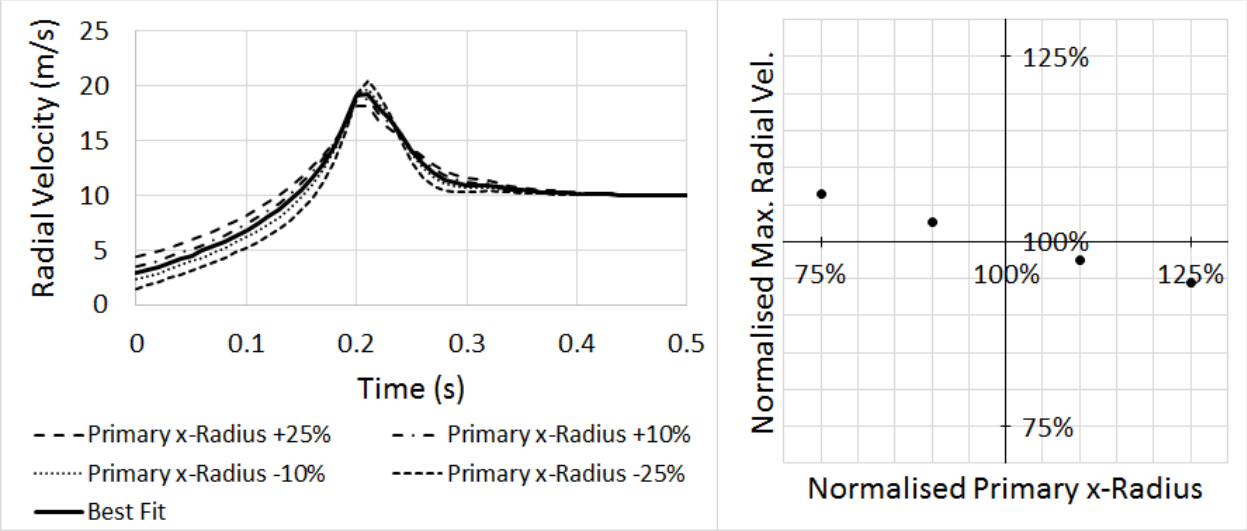

Figure 11: Effect of varying the initial x-radius of the primary vortex. Radial velocity time-series at $x/D = 1.50$ and normalised variation. Normalisation is by the Best Fit value.

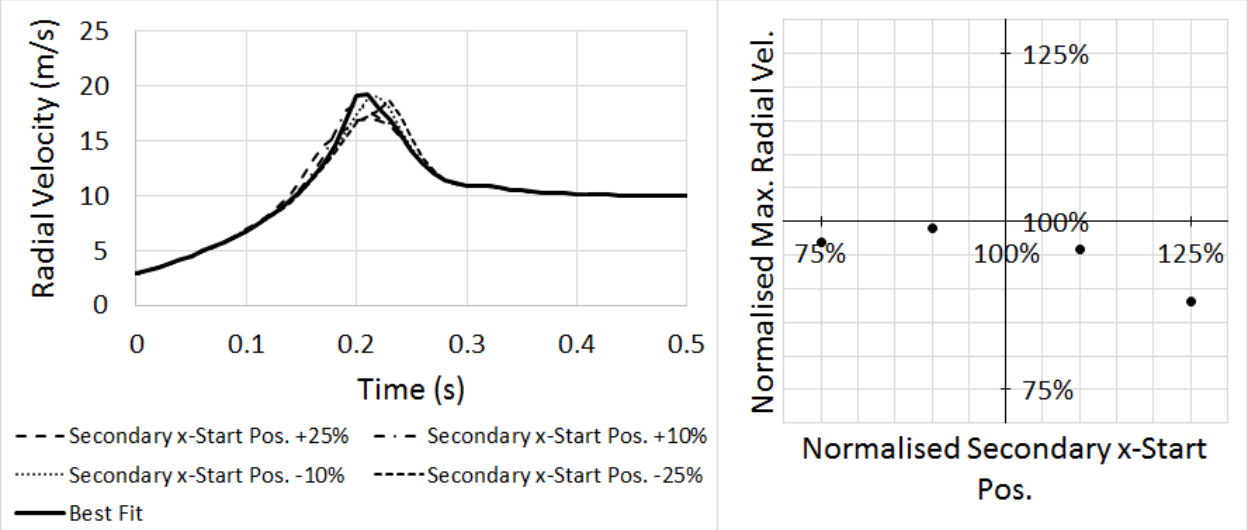

Figure 12: Effect of varying the initial x-start position of the secondary vortex. Radial velocity time-series at $x/D = 1.50$ and normalised variation. Normalisation is by the Best Fit value.

Changing the initial z-radius of the primary vortex does not change x_m but does reduce u_m. in a similar manner to that seen for the secondary vortex x-start position (Figure 13). The base of the time-series peak is also widened as the initial z-radius decreases, and the initial velocity increases. The change in the initial primary z-radius causes assumption (e) (Section 3.2) to no longer hold, and the circumferences of the two vortices to no longer meet. This separation causes a change in the vertical profile of radial velocity (Figure 14) which may account for the stepped shape of the profile nose seen in Figure 5 for $x/D = 1.50$, where there is a sharp deceleration around $z/D = 0.06$. Varying the z start position of the primary vortex has the same effect, as would be expected given the reasons for the changes.

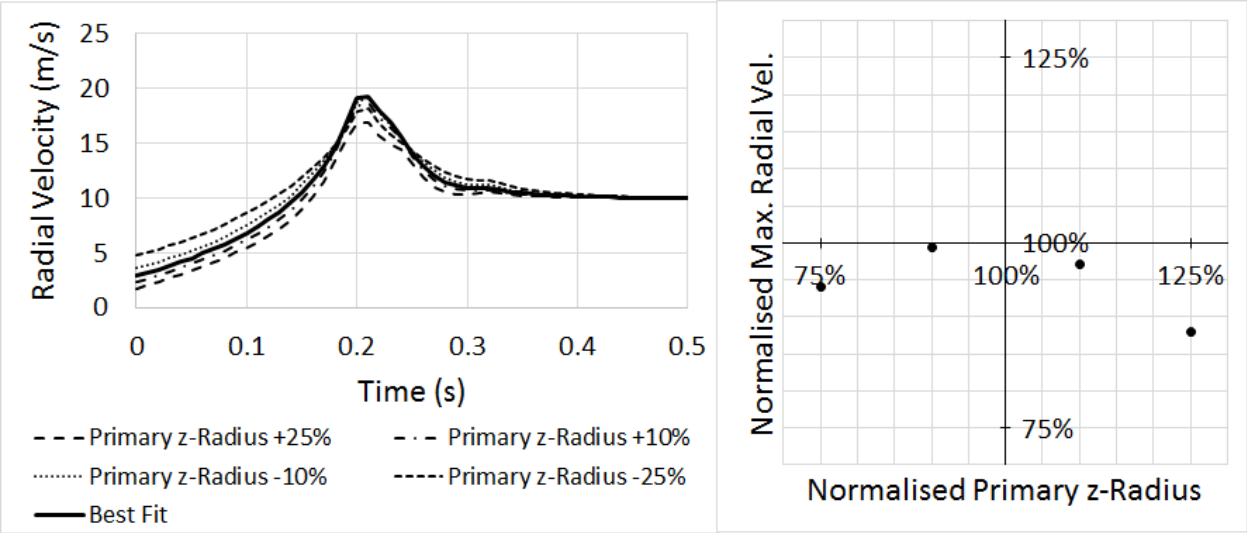

Figure 13: Effect of varying the initial z-radius of the primary vortex. Radial velocity time-series at $x/D = 1.50$ and normalised variation. Normalisation is by the Best Fit value.

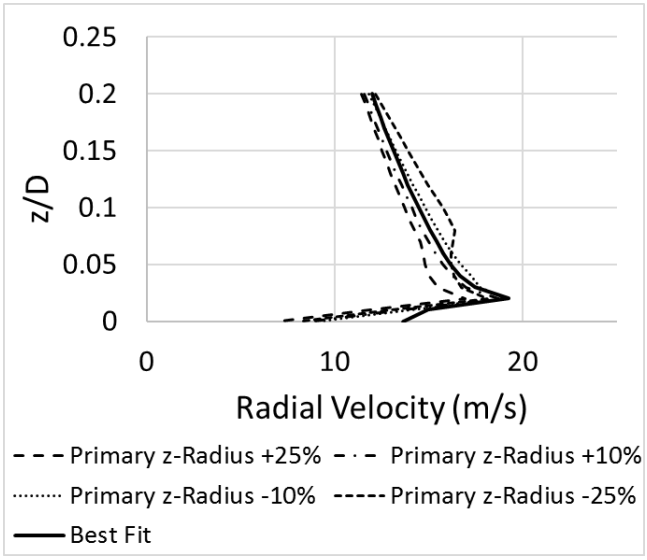

Figure 14: Effect of varying the initial z-radius of the primary vortex. Vertical profile of radial velocity at $x/D = 1.50$ and normalised variation. Normalisation is by the Best Fit value.

5 CONCLUSIONS

In this paper, we have outlined a simple, analytical model which is shown to appropriately capture the main features of a thunderstorm downburst outflow. Both the primary and secondary vortices

associated with downburst flows are modelled. A parametric analysis shows that the maximum wind speed, u_m, varies linearly with initial primary circulation, and has an inverse, linear relationship with rate of decay of the primary vortex. The half-life of the secondary vortex, which forms and then decays once the primary vortex starts to move outwards from the downdraft impingement point, has a more complex, inverse, non-linear relationship with u_m, and also affects the time at which u_m occurs; the relationship between the initial position of the secondary vortex and u_m is more complex still. The shape of the downburst "nose" is shown to be dependent on the vertical separation of the primary and secondary vortices, modelled in the parametric study as a variation of the primary vortex height or vertical starting position.

It is acknowledged that a number of simplifying assumptions have been made along the way which may in the future prove to be unrealistic. Nevertheless, the results are remarkable and offer, for the first time, a computationally inexpensive tool which could be used for design purposes. Random variation of the important parameters may be used to quantify an envelope of possible wind speeds which could be used to inform the design process.

6 ACKNOWLEDGEMENTS

The authors would like to thank the UK Engineering and Physical Science Research Council, which funded the original research on which this model is based under grant number EP/J008281/1.

7 REFERENCES

[1] T. T. Fujita, 'Downburst: Microburst and macroburst', *Univ. Chic. Press IL*, p. pp.-p. 122, 1985.
[2] J. Kim and H. Hangan, 'Numerical simulations of impinging jets with application to downbursts', *J. Wind Eng. Ind. Aerodyn.*, vol. 95, pp. 279–298, 2007.
[3] M. S. Mason, G. S. Wood, and D. F. Fletcher, 'Numerical simulation of downburst winds', *J. Wind Eng. Ind. Aerodyn.*, vol. 97, pp. 523–539, 2009.
[4] T. T. Fujita and R. M. Wakimoto, 'Five scales of airflow associated with a series of downbursts on 16 July 1980', *Mon. Weather Rev.*, vol. 109, pp. 1439–1456, 1981.
[5] M. R. Hjelmfelt, 'Structure and life cycle of microburst outflows observed in Colorado', *J. Appl. Meteorol.*, vol. 27, no. August, pp. 900–927, 1988.
[6] E. C. C. Choi, 'Field measurement and experimental study of wind speed profile during thunderstorms', *J. Wind Eng. Ind. Aerodyn.*, vol. 92, pp. 275–290, 2004.
[7] F. T. Lombardo, 'Thunderstorm characteristics of wind engineering importance', presented at the In Proceedings of the 13th International Conference on Wind Engineering, 2011.
[8] F. T. Lombardo, D. A. Smith, J. L. Schroeder, and K. C. Mehta, 'Thunderstorm characteristics of importance to wind engineering', *J. Wind Eng. Ind. Aerodyn.*, vol. 125, no. 0, pp. 121–132, 2014.
[9] K. Butler and A. Kareem, 'Physical and numerical modeling of downburst generated gust fronts', presented at the Proceedings of the 12th International Conference on Wind Engineering, Cairns, Australia, 2007, pp. 791–798.

[10] M. T. Chay and C. W. Letchford, ‘Pressure distributions on a cube in a simulated thunderstorm downburst - Part A: stationary downburst observations’, *J. Wind Eng. Ind. Aerodyn.*, vol. 90, no. 7, pp. 711–732, 2002.
[11] M. T. Chay and C. W. Letchford, ‘Pressure distributions on a cube in a simulated thunderstorm downburst - Part B: moving downburst observations’, *J. Wind Eng. Ind. Aerodyn.*, vol. 90, no. 7, pp. 733–753, 2002.
[12] M. Jesson, M. Sterling, C. Letchford, and C. Baker, ‘Aerodynamic forces on the roofs of low-, mid- and high-rise buildings subject to transient winds’, *J. Wind Eng. Ind. Aerodyn.*, vol. 143, no. 0, pp. 42–49, 2015.
[13] M. Jesson, M. Sterling, C. Letchford, and M. Haines, ‘Aerodynamic forces on generic buildings subject to transient, downburst-type winds’, *J. Wind Eng. Ind. Aerodyn.*, vol. 137, no. 0, pp. 58–68, 2015.
[14] T. S. Lundgren, J. Yao, and N. N. Masour, ‘Microburst modelling and scaling’, *J. Fluid Mech.*, vol. 239, pp. 461–488, 1992.
[15] L. G. Orf, C. Oreskovic, E. Savory, and E. Kantor, ‘Circumferential analysis of a simulated three-dimensional downburst-producing thunderstorm outflow’, *J. Wind Eng. Ind. Aerodyn.*, vol. 135, no. 0, pp. 182–190, 2014.
[16] B. C. Vermeire, L. G. Orf, and E. Savory, ‘Improved modelling of downburst outflows for wind engineering applications using a cooling source approach’, *J. Wind Eng. Ind. Aerodyn.*, vol. 99, no. 8, pp. 801–814, 2011.
[17] A. C. McConville, M. Sterling, and C. J. Baker, ‘The physical simulation of thunderstorm downbursts using an impinging jet’, *Wind Struct.*, vol. 12, no. 2, pp. 133–149, 2009.
[18] J. D. Holmes and S. E. Oliver, ‘An empirical model of a downburst’, *Eng. Struct.*, vol. 22, pp. 1167–1172, 2000.
[19] M. Jesson and M. Sterling, ‘A Simple Vortex Model of a Thunderstorm Downburst’, presented at the 12th UK Conference on Wind Engineering, 2016.
[20] M. R. Haines, ‘The simulation of non-synoptic effects and their implications for engineering structures’, University of Birmingham, UK, Birmingham, 2015.